KSCE Journal of Civil Engineering
DOI 10.1007/s12205-024-0559-9

pISSN 1226-7988, eISSN 1976-3808
www.springer.com/12205

Structural Engineering

Comparative Study on CNN-based Bridge Seismic Damage Identification Using Various Features

Xiaohang Zhou[a], **Yian Zhao**[a], **Inamullah Khan**[b], **and Lu Cao**[a]

[a]*School of Civil Engineering and Architecture, Guangxi University, Nanning 530004, China*
[b]*National Institute of Transportation, National University of Science and Technology, Islamabad 44000, Pakistan*

ARTICLE HISTORY

Received 20 March 2024
Revised 8 June 2024
Accepted 10 July 2024
Published Online 5 September 2024

KEYWORDS

Continuous rigid bridge
Seismic damage
Damage identification
Damage feature
Convolutional neural network

ABSTRACT

Quick and accurate identification of bridge damage after an earthquake is crucial for emergency decision-making and post-disaster rehabilitation. The maturing technology of deep neural networks (DNN) and the integration of health monitoring systems provide a viable solution for seismic damage identification in bridges. However, how to construct damage features that can efficiently characterize the seismic damage of the bridge and are suitable for the use with DNN needs further investigation. This study focuses on seismic damage identification for a continuous rigid bridge using raw acceleration responses, statistical features, frequency features, and time-frequency features as inputs, with damage states as outputs, employing a deep convolutional neural network (CNN) for pattern classification. Results indicate that all four damage features can identify seismic damage, with time-frequency features achieving the highest accuracy but having a complex construction process. Frequency features also demonstrate high accuracy with simpler construction. Raw acceleration response and statistical features perform poorly, with statistical features deemed unsuitable as damage indicators. Overall, frequency features are recommended as CNN inputs for quick and accurate bridge seismic damage identification.

1. Introduction

Earthquakes are highly impactful natural disasters that can cause significant damage to transportation infrastructure. As critical transportation network components, bridges in earthquake-prone areas are particularly vulnerable to earthquake damage. While direct casualties resulting from earthquake damage to bridges are generally limited, the ensuing traffic disruption will significantly impede subsequent earthquake relief efforts, and the resulting indirect losses are challenging to quantify accurately. Thus, it is of utmost importance to determine the seismic damage status of bridges promptly and accurately, providing a crucial foundation for emergency management decisions and post-earthquake rehabilitation (Ni et al., 2015).

Seismic waves carry substantial energy, resulting in a complex state of bridge damage during seismic excitation. The response exhibits non-stationary and nonlinear characteristics (Cao and Friswell, 2009). Furthermore, a coupling relationship exists between changes in the bridge's damage state and the characteristics of the seismic excitation, which jointly influence the bridge's response. Additionally, the bridge's low-order modes are densely distributed, contributing to a low signal-to-noise ratio in the response. These challenging factors pose difficulties in accurately identifying seismic damage in bridges. Therefore, the key to accurately identifying bridge seismic damage lies in decoupling the damage state and seismic excitation characteristics from the non-stationary and nonlinear response while effectively extracting the features that reflect the bridge's damage state. Scholars have conducted extensive research to develop suitable damage features for bridge seismic damage identification. Li et al. (2019) established a finite element model of a curved beam bridge for seismic damage identification. They used wavelet packet transformation on displacement responses and wavelet packet singular entropy to construct damage features, enabling precise identification of damage locations. Deng et al. (2021) developed a finite element model of a curved beam bridge under seismic excitation and obtained its displacement response. They used wavelet packet transformation to decompose the displacement response and

CORRESPONDENCE Xiaohang Zhou zhou@gxu.edu.cn School of Civil Engineering and Architecture, Guangxi University, Nanning 530004, China

constructed damage features based on wavelet packet norm entropy. By analyzing the mutation position of the damage index curve, they identified the damage location and evaluated its severity based on the mutation peak. Liu et al. (2023) established a finite element model of a cable-stayed bridge and simulated seismic excitation to obtain the structural strain response. They used the transmissibility function to address different excitations and identified damage locations by analyzing the energy change in the structural strain response before and after damage. To validate their approach, they also developed a cable-stayed bridge test model.

In the studies mentioned earlier, seismic damage identifications of bridges were performed by artificially constructing damage indicators. However, the manual extraction method entails laborious efforts, and its applicability has yet to be extensively validated. In recent years, the Deep Neural Network (DNN) has experienced rapid advancement owing to its remarkable feature extraction capabilities, enabling end-to-end learning for practical problem-solving without reliance on prior human knowledge. This makes it well-suited for addressing intricate and nonlinear problems. Consequently, civil engineering has witnessed extensive utilization of DNN for structural damage identification purposes. Zhang et al. (2019) used experimental simulations to obtain bridge acceleration responses, which served as input for a 1-dimensional convolutional neural network(1D-CNN) to detect subtle changes in structural mass and stiffness. Teng et al. (2020) constructed an experimental model of a steel truss bridge and stimulated it using a force hammer, and the acceleration responses are used as inputs for a 1D-CNN to identify the damage location of the bridge. Zou et al. (2021) developed a scale model of a three-span continuous rigid bridge. They used a hand-pulled trolley to simulate vehicle loads and obtained acceleration responses as input for the neural network. By combining a CNN with a gated recurrent neural network (RNN), they effectively assessed the damage degree of the bridge model. Zhang et al. (2022) developed a steel truss bridge test model and subjected it to impact from a hammer. They recorded the acceleration and strain responses, which were fused and input into a CNN to accurately identify the location and extent of damage in the bridge.

However, previous studies have indicated that the accuracy of structural damage identification using deep learning is not significantly high when the collected response signal is directly employed as the input for the network. Recognizing this concern, numerous researchers have endeavored to conduct further investigations on this matter. He et al. (2021a) established a finite element model of a three-span continuous reinforced concrete girder bridge. They employed wavelet packets to filter and reconstruct the structural response obtained from the vehicle-bridge coupling vibration. Recursive analysis was utilized to generate damage features from the obtained recursive graphs. A convolutional neural network was then employed to identify the location and degree of structural damage. He et al. (2021b) developed a three-layer frame structure experimental model. The structure was stimulated to obtain the acceleration response, and a fast Fourier transform was employed to extract frequency information. The damage degree of the frame structure was identified using a deep convolutional neural network. Furthermore, a comparison with traditional machine learning algorithms demonstrated the higher identification accuracy achieved by the proposed method. Wu et al. (2022) developed a finite element model of a simply supported steel beam and used a force hammer to obtain the acceleration response. They performed wavelet packet decomposition on the response to construct damage features based on changes in energy ratios across frequency bands, and a CNN was used to identify the damage location. The method was validated with a test model, showing that frequency domain and time-frequency domain transformations of the response signal led to improved identification accuracy when used as neural network input. However, it is important to note that this approach necessitates significant computational and time investments, thus hindering the timely identification of seismic damage.

Bridge seismic damage identification is a subset of structural damage identification but is more complex due to pronounced nonlinearity and non-stationarity in its response. DNN holds significant theoretical potential for this task, yet the literature remains limited. This study aims to discover features that accurately reflect bridge damage under seismic conditions, minimizing the need for complex manual intervention. The ultimate goal is to rapidly identify earthquake-induced bridge damage.

This paper presents a comparative analysis of various damage features utilizing deep CNNs. The underlying framework is visually depicted in Fig. 1. The subsequent sections of this article are structured as follows: Section 2 outlines the seismic damage simulation methodology for the continuous rigid bridge. Section 3 describes the extraction process for acceleration, statistical,

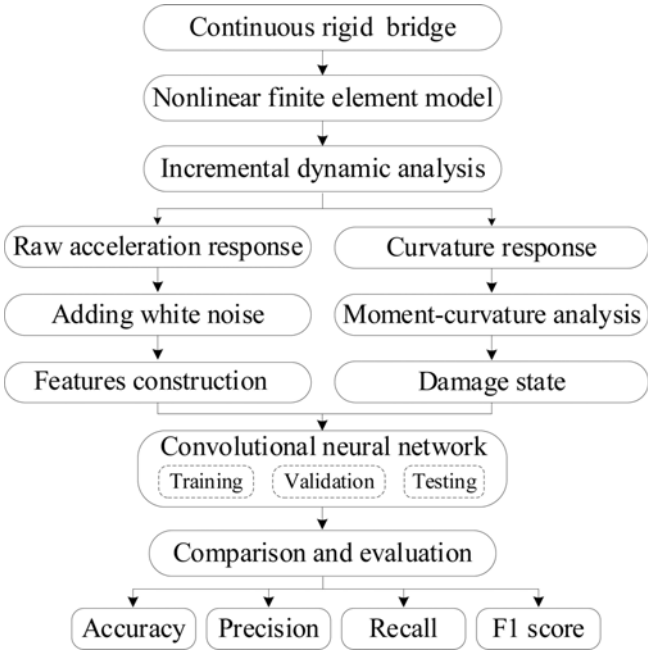

Fig. 1. Framework of Bridge Seismic Damage Identification

frequency domain, and time-frequency domain features. Section 4 provides detailed information regarding the construction of CNN. Finally, Section 5 delves into a comprehensive discussion of the results obtained from damage identification using different features.

2. Seismic Damage Simulation

2.1 Bridge Model

The bridge has a total length of 650 m, with a span arrangement consisting of segments measuring 80 m, 130 m, 2 × 170 m, and 100 m. The heights of the piers numbered 1, 2, 3, and 4 are 26.9 m, 123.54 m, 91.63 m, and 80.14 m, respectively. The main girder features a single box and single chamber variable section constructed with C50 concrete. The piers are hollow rectangular sections composed of C40 concrete and HRB 335 reinforcement. The overall arrangement of the continuous rigid bridge is shown in Fig. 2.

2.2 Finite Element Model Establishing

The finite element model of the continuous rigid bridge is developed utilizing the Open System for Earthquake Engineering Simulation (OpenSees) software. In seismic events, the bridge pier is prone to greater vulnerability than the main girder structure, typically exhibiting plastic deformation prior to the main girder structure. Consequently, this study employs an elastic beam-column element to represent the main girder, a nonlinear beam-column element to emulate the bridge pier, and a zero-length element to simulate the bidirectional movable bearing.

Previous research on bridge disasters following earthquakes has identified key components vulnerable to seismic damage, including foundations, supports, and piers (Chiou et al., 2019; Jiao et al., 2019; Lu et al., 2019). Among these components, piers are particularly susceptible to seismic damage. Consequently, the condition of the piers can serve as an indirect indicator of the overall damage state of a continuous rigid bridge (Shinozuka et al., 2000). Therefore, it is imperative to effectively simulate the nonlinear motion mechanism of bridge piers when subjected to seismic forces, as this will enable the accurate assessment of seismic response to identify and evaluate bridge seismic damage.

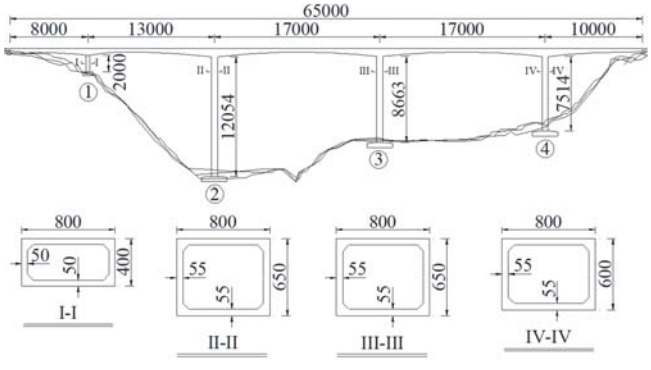

Fig. 2. Overall Arrangement of the Bridge

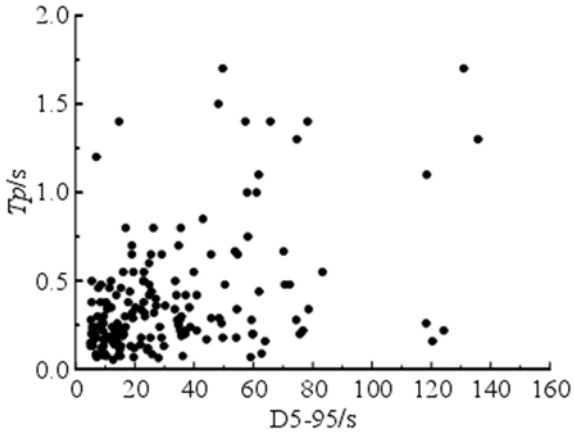

Fig. 3. Characteristic Distribution of Ground Motions

This paper utilizes nonlinear beam-column elements and fiber sections to simulate the behavior of the piers accurately. For the fiber section definition, three distinct materials represent the piers: protective layer concrete, core area concrete, and steel bars. The concrete and confined concrete are simulated with the modified Kent-Park model (Scott et al., 1982), and the steel bars are simulated with the Johnson-Cook model (Johnson and Cook, 1983).

2.3 Incremental Dynamic Analysis

The characteristics of seismic excitation significantly influence the seismic damage state of the bridge (Zhou et al., 2013). To enrich the seismic damage state of the continuous rigid bridge, it is essential to consider the inherent randomness and discreteness of seismic waves. For this purpose, 155 different ground motion records were selected from the PEER ground motion database. Fig. 3 depicts the characteristic distribution of these selected records. Peak ground acceleration (PGA) is used as the ground motion intensity index. Then, Incremental Dynamic Analysis (IDA) was used to conduct the seismic damage analysis. Considering that weak ground motion may not cause seismic damage to the bridge, the selected records were adjusted from 0.1 g to 0.5 g with an incremental step of 0.1 g. Consequently, 775 seismic waves were generated for the subsequent IDA.

Before employing a deep CNN for damage identification, it is imperative to ascertain that the inputs possess consistent feature dimensions. As a result, it becomes essential to standardize the durations of all ground motions before executing an incremental dynamic analysis on the continuous rigid bridge. The established continuous rigid bridge exhibits a base period of 4.13s. In order to fulfill the requirement that ground motion durations range from 5 to 10 times the basic period of the structure, the durations of all ground motions are adjusted to 40s.

2.4 Damage Definition

The moment-curvature analysis is conducted on both the upper and lower sections of each pier. The resulting curvature serves as an indicator for assessing the extent of pier damage, which is

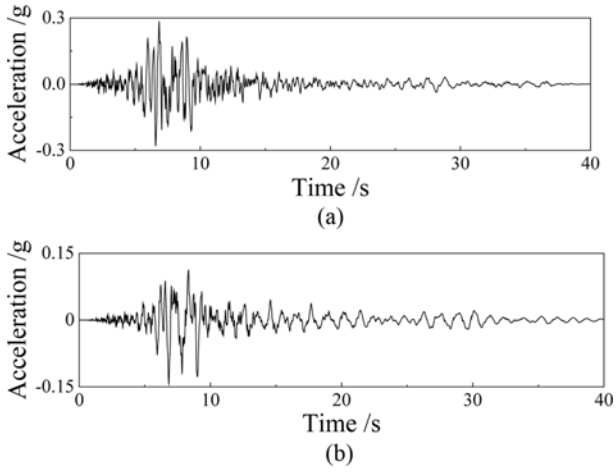

Fig. 4. Excitation and Response: (a) Seismic Waveform, (b) Acceleration Response

Table 1. Seismic Damage State of Piers

Location	PGA/g				
	0.1	0.2	0.3	0.4	0.5
#1 Top	SD	GD	CD	CD	CD
#1 Bottom	ND	GD	CD	CD	CD
#2 Top	ND	ND	ND	ND	MD
#2 Bottom	ND	ND	ND	ND	MD
#3 Top	ND	ND	ND	SD	GD
#3 Bottom	ND	ND	ND	ND	MD
#4 Top	ND	ND	SD	MD	GD
#4 Bottom	ND	ND	MD	GD	GD

categorized into five distinct states: no damage (ND), slight damage (SD), moderate damage (MD), grave damage (GD), and complete damage (CD).

This paper uses the record of LOMAP as an example to demonstrate the definition of seismic damage state of the bridge. The acceleration waveform of the LOMAP is presented in Fig. 4(a), while Fig. 4(b) displays the acceleration response at the top of Pier #1 for an excitation with PGA = 0.1 g. the corresponding damage states of piers are summarized in Table 1.

3. Feature Engineering

The pivotal aspect of bridge seismic damage identification lies in extracting features that accurately depict the seismic damage condition of the bridge. Accordingly, this section provides a comprehensive account of establishing statistical, frequency, and time-frequency features. The acceleration response in Fig. 4(b) is employed to illustrate the feature Engineering. It should be pointed out that the samples used for subsequent damage identification are identical, including the training, validation, and testing of different networks. Four types of damage features are extracted from these samples to study their ability to characterize the damage state of bridges under seismic excitation.

3.1 Acceleration Response

The acceleration responses of the eight measuring points are interconnected in parallel, corresponding to the top and bottom sections of Piers #1 to #4. Since the adjusted seismic wave data length is 4000, the sample with a data dimension of 4000 rows and eight columns is obtained, as depicted in Fig. 4(b).

3.2 Statistical Features

Statistical features belong to a category of time-domain features that describe the distribution and change trend of the signal. In practical applications, the selection of specific statistical features for analysis depends on the data characteristics and task requirements. These features commonly serve as inputs for machine learning models employed in damage identification tasks. Common statistical features encompass the mean, variance, standard deviation, median, skewness and kurtosis.

In mathematics and statistics, moments serve as measures for evaluating a variable's distribution and morphological characteristics. Specifically, the nth-order moment is computed by integrating the product of the nth power of the variable and its corresponding probability density function (Spokoiny and Dickhaus, 2015). The 1st to 4th moments of a data series are defined as mean, variance, skewness, and kurtosis, respectively.

The mean, a fundamental statistical measure, represents the central tendency of a dataset, calculated as the average of all data points. Variance quantifies the extent of dispersion among data points. The greater the variance, the greater the degree of dispersion of the data. Skewness is a statistical measure that describes the asymmetry of a data distribution, while kurtosis measures the degree of spikes in the data distribution. Thus, the mean, variance, skewness, and kurtosis of the acceleration responses are employed as fundamental statistical indices to construct the statistical damage feature. The construction process encompasses the following steps:

1. The acceleration response is partitioned into 20 distinct intervals, each corresponding to a specific percentage of the total acceleration response time, ranging from 5% to 95%. The mean, variance, skewness, and kurtosis are computed independently for each basic interval.
2. Subsequently, the mean, variance, skewness, and kurtosis values obtained from the 20 basic intervals are concatenated sequentially to form a feature vector for each measurement point. Since there are 8 test channels, a resulting sample possesses a data dimension of 80 rows and eight columns.

As an illustrative example, the mean value, variance, skewness and kurtosis of the acceleration response at the top of Pier 1# are presented in Figs. 5(a) to 5(d), respectively.

3.3 Frequency Features

Frequency analysis converts time-domain signals into the frequency domain, with the Fast Fourier Transform (FFT) commonly used for discrete frequency analysis. The FFT can reduce the number of calculations from N^2 to $N \cdot \log_2 N$ through a divide-and-conquer strategy and butterfly operation, where N is the number of data

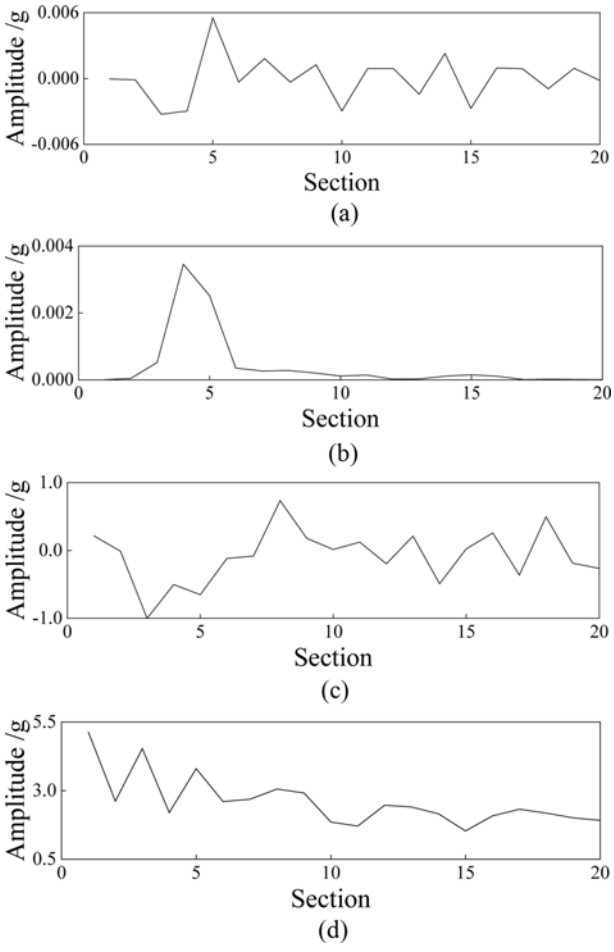

Fig. 5. Statistical Features of Acceleration Response: (a) Mean, (b) Variance, (c) Skewness, (d) Kurtosis

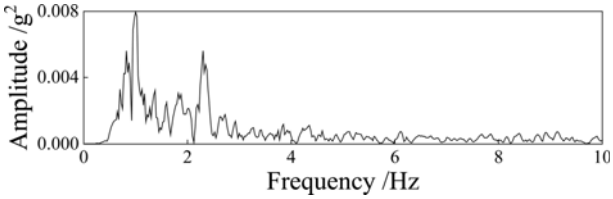

Fig. 6. Fourier Spectrum of Acceleration

points. Consequently, this significantly reduces the computational complexity, thereby enabling efficient spectrum analysis.

As the frequency range associated with the initial ten modes of the continuous rigid bridge remains below 10 Hz, this study selectively focuses on the amplitude values corresponding to the frequency range up to 10 Hz to construct the frequency damage feature. Consequently, eliminating redundant and irrelevant data is theoretically expected to increase identification accuracy. The corresponding Fourier spectrum is shown in Fig. 6. Therefore, the sample data dimension is 400 rows and eight columns.

3.4 Time-Frequency Features

The time-frequency analysis investigates signal characteristics in both time-domain and frequency-domain. Thus, rich structural state information is revealed in its decomposition results. In this study, the Variational Mode Decomposition (VMD) algorithm has been chosen to decompose the acceleration responses.

The performance of VMD mainly depends on the number of modal components (k), and the penalty factor (α). Selecting appropriate values for these parameters is crucial for optimal decomposition. If k is too small, the decomposition will be

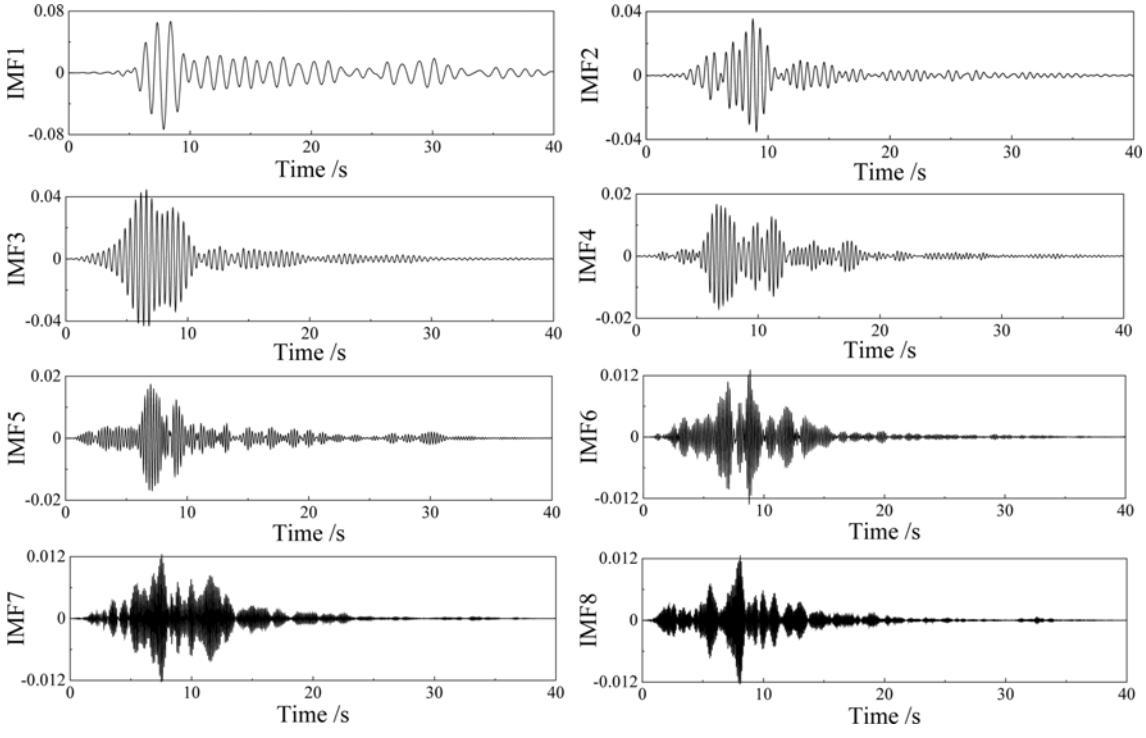

Fig. 7. VMD Results of the Acceleration Response

insufficient, causing mode aliasing. Conversely, if k is too large, over-decomposition occurs. Similarly, α influences decomposition quality: a small α may lead to mode aliasing by mixing signals from other components, while a large α may result in the loss of useful information. In this study, we set $k = 8$ and $\alpha = 10000$.

Figure 7 shows the VMD decomposition results of the acceleration in Fig. 4(b). The first five Intrinsic Mode Functions (IMFs) are used to construct the time-frequency features, resulting in a sample data dimension of 4000 rows and 40 columns.

4. Establishment of CNN

4.1 Network Architecture

A CNN consists of essential components such as the input layer, convolutional layer, max pooling layer, flattening layer, fully connected layer, and output layer. The optimal network architecture is typically determined by the complexity of the specific target task. After comparing different layer combinations, a comprehensive network architecture is established to accommodate variations in diverse datasets. The fundamental CNN architecture is depicted in Fig. 8.

4.2 Sample Augmentation

In practical engineering scenarios, acquiring adequate samples is often constrained. Data augmentation is an effective solution to address this limitation and enhance model performance while mitigating the risk of network overfitting. In this study, we employed data augmentation techniques to augment the available seismic damage samples of the continuous rigid bridge. Specifically, we added random Gaussian white noise with a signal-to-noise ratio of 10 to the original acceleration samples, resulting in 1550 augmented sample sets. These sets were then partitioned into a training set and a test set, with a ratio of 0.8:0.2. Furthermore, to ensure optimal model generalization, 20% of the samples from the training set were further allocated to a validation set.

4.3 Optimal Network Selection

During the learning process, the performance of the network does not always improve continuously. Excessive training can lead to decreased performance on the validation set, indicating overfitting. To address this issue, the network's performance is monitored throughout training, and its parameters are saved at each epoch. Once training is completed, the parameters from the epoch with the highest validation accuracy are selected as the optimal network. This strategy ensures the best generalization on unknown samples while avoiding the impact of manually setting the epoch number, as demonstrated in Fig. 9.

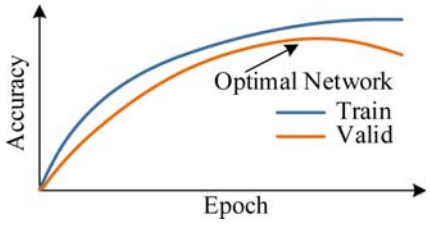

Fig. 9. Optimal Network Selection

4.4 Hyperparameter Settings

In this paper, Leaky ReLU (Maas et al., 2013) is chosen as the activation function, and its functional form is $f(x) = \max(ax, x)$. Leaky ReLU addresses the vanishing gradient problem associated with the left side of ReLU, thereby reducing model complexity and improving computational efficiency. Since bridge seismic damage identification is a multi-classification problem, the Softmax function (Grave et al., 2017) is used as the network's classification function. Mean Squared Error (MSE) is selected as the loss function to evaluate the discrepancy between the actual labels and the predicted labels (Chicco et al., 2021).

The Adam algorithm is used for adaptive learning rate optimization. It dynamically adjusts the learning rate through gradient first-order and second-order moment estimation, making it particularly suitable for scenarios with numerous parameters. The parameters of the Adam algorithm are set as follows: $lr = 0.001$, $\beta_1 = 0.9$, $\beta_2 = 0.999$, $\varepsilon = 1E\text{-}08$. The batch size is set to 64 while the number of epochs is 1000.

5. Seismic Damage Identification

In this section, four networks are trained on acceleration, statistical features, frequency features, and time-frequency features. The networks share the same architecture, as shown in Fig. 8, with varying widths based on feature lengths. During training, losses and accuracies are tracked to select the optimal parameter combination. After training, the best-performing parameters are retained, and the test samples are used to obtain prediction results, completing the seismic damage identification. The effectiveness of the damage features is comprehensively assessed using four evaluation metrics: accuracy, precision, recall, and F1 score

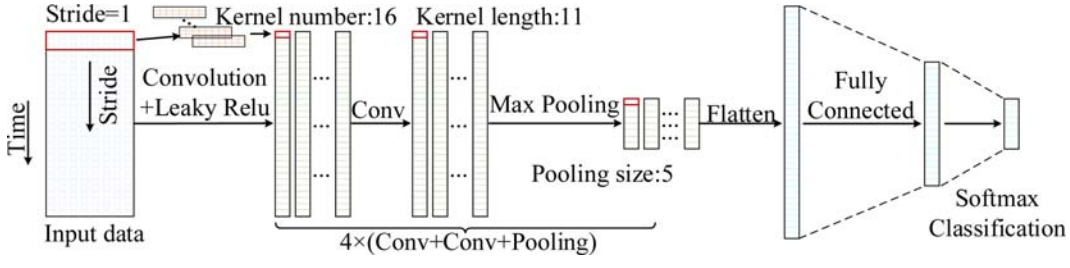

Fig. 8. Basic Architecture of CNN

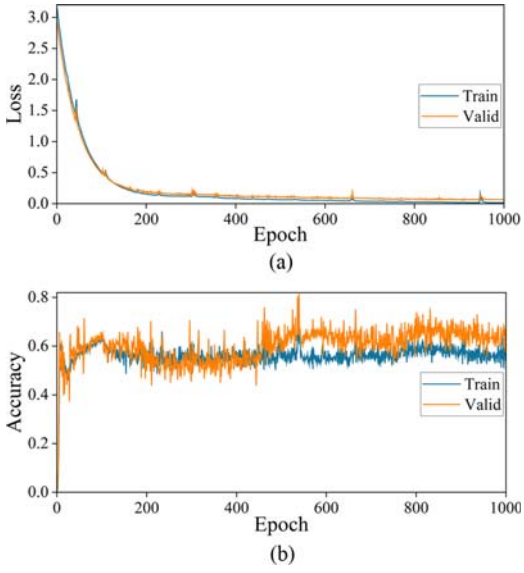

Fig. 10. Tracking of Training and Validation on Acceleration: (a) Loss, (b) Accuracy

(Sokolova and Lapalme, 2009).

5.1 Results of Raw Acceleration

The loss and accuracy of the network trained on raw acceleration data are demonstrated in Fig. 10.

Confusion matrices are used to display the detailed damage identification results for each location, as shown in Fig. 11, with precisions and recall rates calculated at the bottom right corner. In subsequent identification results, the comprehensive accuracies will be presented instead of confusion matrices.

Table 2. Accuracy on Acceleration

Location	Accuracy	Location	Accuracy
#1 Top	95.45%	#3 Top	96.75%
#1 Bottom	96.43%	#3 Bottom	95.78%
#2 Top	97.08%	#4 Top	96.10%
#2 Bottom	94.16%	#4 Bottom	95.13%

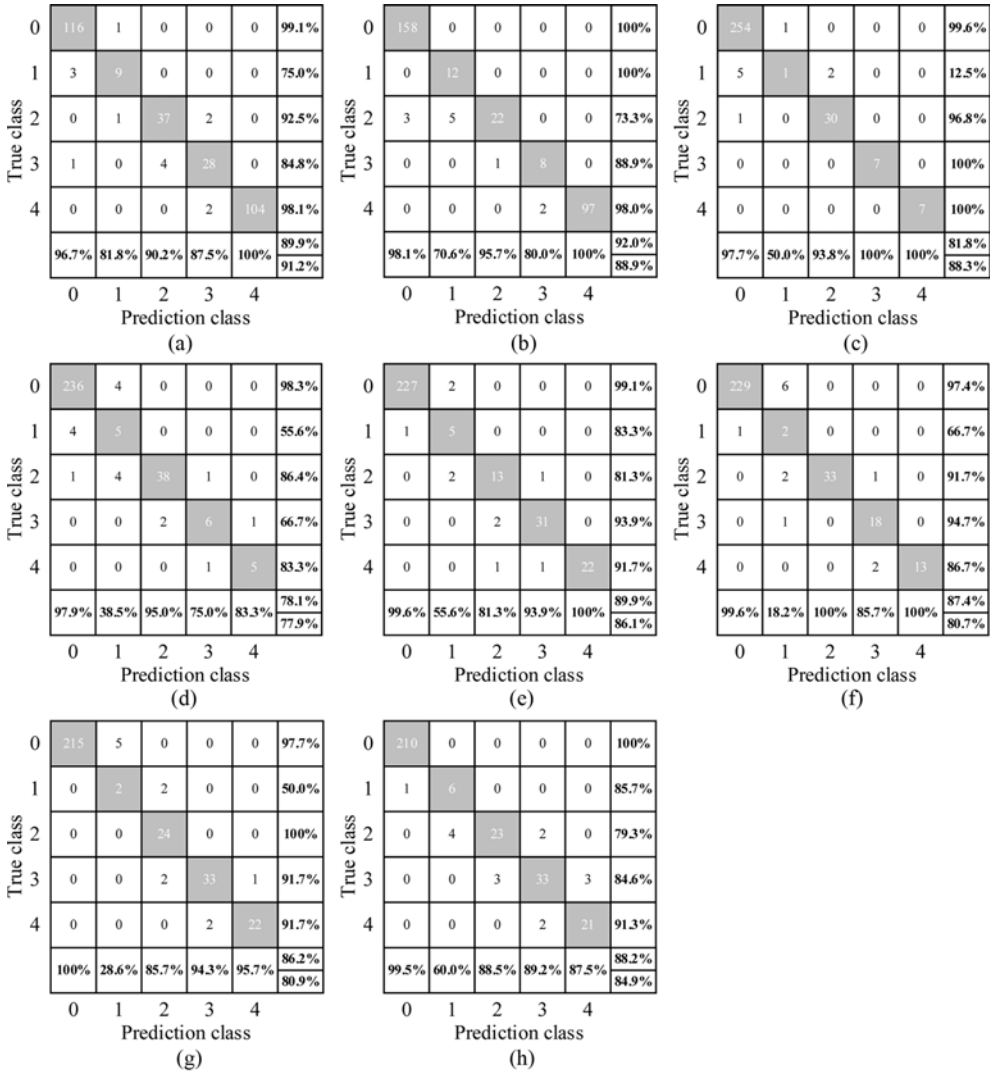

Fig. 11. Confusion Matrix Based on Acceleration: (a) Pier #1 Top, (b) Pier #1 Bottom, (c) Pier #2 Top, (d) Pier #2 Bottom, (e) Pier #3 Top, (f) Pier #3 Bottom, (g) Pier #4 Top, (h) Pier #4 Bottom

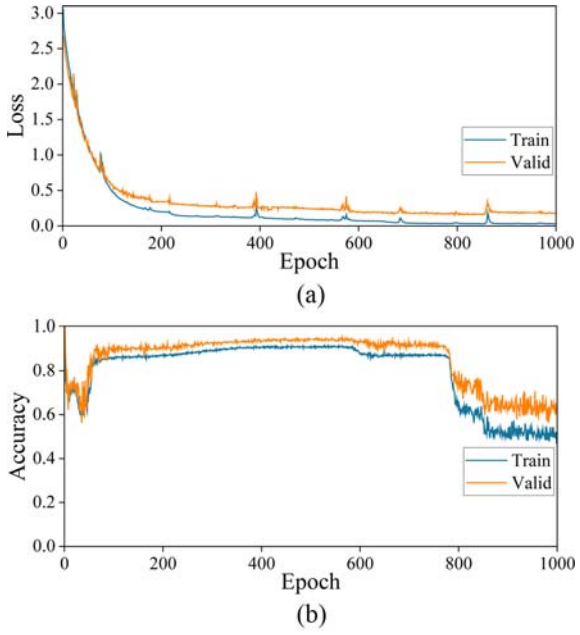

Fig. 12. Tracking of Training and Validation on Statistical Features: (a) Loss, (b) Accuracy

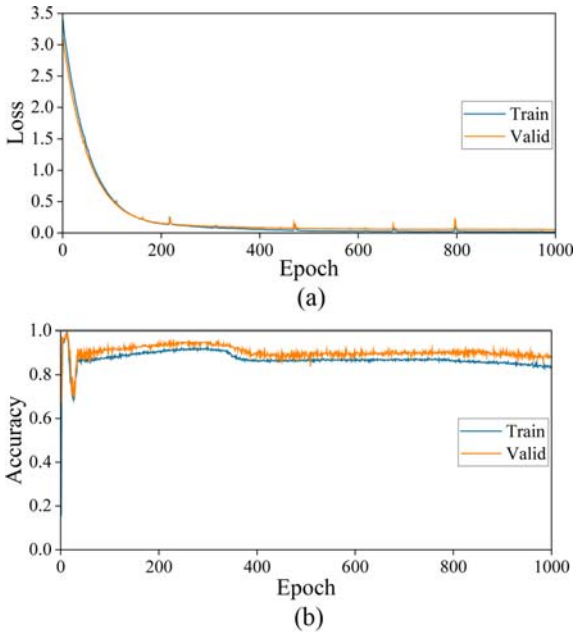

Fig. 13. Tracking of Training and Validation on Frequency Features: (a) Loss, (b) Accuracy

Table 3. Accuracy on Statistical Features

Location	Accuracy %	Location	Accuracy %
#1 Top	88.31	#3 Top	93.18
#1 Bottom	92.86	#3 Bottom	93.51
#2 Top	94.48	#4 Top	92.53
#2 Bottom	92.86	#4 Bottom	93.51

Table 4. Accuracy on Frequency Features

Location	Accuracy %	Location	Accuracy %
#1 Top	95.78	#3 Top	95.13
#1 Bottom	96.43	#3 Bottom	97.40
#2 Top	98.38	#4 Top	95.78
#2 Bottom	94.81	#4 Bottom	98.70

According to Fig. 11, the identification accuracies for each location are calculated, as shown in Table 2.

5.2 Results of Statistical Features

The loss and accuracy of the network trained on statistical features are demonstrated in Fig. 12.

The corresponding identification accuracies for each location are calculated, as shown in Table 3.

5.3 Results of Frequency Features

The loss and accuracy of the network trained on frequency features are demonstrated in Fig. 13.

The corresponding identification accuracies for each location are calculated, as shown in Table 4.

5.4 Results of Time-Frequency Features

The loss and accuracy of the network trained on time-frequency features are demonstrated in Fig. 14.

The corresponding identification accuracies for each location are calculated, as shown in Table 5.

To compare the effectiveness of different damage features, the F1 score is employed as a comprehensive metric. This metric considers both the precision and recall rate of the identification results, providing a holistic evaluation of network performances. The corresponding F1 scores for the damage identification results of

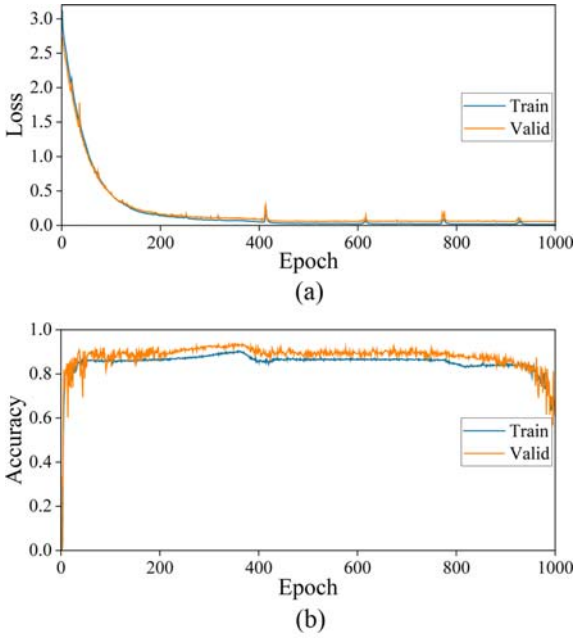

Fig. 14. Tracking of Training and Validation on Time-frequency Features: (a) Loss, (b) Accuracy

Table 5. Accuracy on Time-Frequency Features

Location	Accuracy %	Location	Accuracy %
#1 Top	94.81	#3 Top	97.73
#1 Bottom	96.43	#3 Bottom	98.05
#2 Top	99.35	#4 Top	97.08
#2 Bottom	99.03	#4 Bottom	96.75

Table 6. F1 Scores Corresponding to Different Feature Identification Results

Damage feature	Acceleration %	Statistical Features %	Frequency Features %	Time-frequency Features %
#1 Top	90.5	76.4	92.1	91.3
#1 Bottom	90.4	73.7	87.2	90.7
#2 Top	84.9	66.2	94.0	97.6
#2 Bottom	78.0	71.7	82.7	97.2
#3 Top	88.0	82.3	86.7	92.7
#3 Bottom	83.9	77.4	83.4	87.8
#4 Top	83.5	80.1	83.5	84.7
#4 Bottom	86.5	81.8	95.9	90.0

four types of damage features are presented in Table 6.

Table 6 reveals that the damage identification results from the time-frequency features outperform the other three features. Notably, the F1 score of 91.3% for the bottom of Pier #1 is slightly lower than the F1 score of 92.1% obtained from the frequency features. Similarly, the F1 score of 90.0% for the bottom of Pier #4 is lower than the F1 score of 95.9% achieved through the frequency features. However, substantial improvements are observed in the F1 scores at the remaining positions. For instance, the F1 scores for the top of Pier #2 based on acceleration, statistical feature, and frequency features are 84.9%, 66.2%, and 94.0%, respectively, whereas the F1 score using the time-frequency features reaches 97.6%. Similarly, the F1 scores for the bottom of Pier #2 based on acceleration, statistical feature, and frequency features are 78.0%, 71.7%, and 82.7%, respectively, whereas the F1 score using the time-frequency features reaches 97.2%.

5.5 Discussions

Based on the results presented in Tables 2 to 5, the comprehensive identification accuracies for the eight piers using acceleration, statistical features, frequency features, and time-frequency features are 95.86%, 92.66%, 96.55%, and 97.40%, respectively. A detailed comparison of the identification accuracies for each section of the eight piers reveals that:

1. All four types of features generally achieved high seismic damage identification accuracies. However, the accuracies for identifying slight damage are relatively low, particularly for the damage at the bottom of Pier #3 and the top of Pier #4. The main reasons for this issue are the small number of samples with slight damage and their tendency to be confused with the no damaged state, as demonstrated in Fig. 11.
2. Seismic excitation causes a distinctive damage pattern in the four piers of the continuous rigid bridge, with damage severity following the sequence: Pier #1 > Pier #4> Pier #3 > Pier #2. Taller piers are less likely to experience seismic damage, leading to an imbalance in the distribution of seismic damage samples. Pier #2 is usually in an undamaged state, making it easier to identify, thus achieving the highest identification accuracy.
3. Time-frequency features generally yield higher identification accuracies compared to other features. However, the identification results for time-frequency features show some undetected damage samples at certain locations, reflected in F1 scores that do not always achieve the highest values. Another drawback of time-frequency features is their complex construction.

6. Conclusions

Based on the seismic damage identification results of the continuous rigid bridge model, the following conclusions are drawn:

1. Bridge seismic damage identification based on vibration tests and CNN is feasible, but the form of input significantly affects the identification accuracy.
2. Among the four types of damage features, the time-frequency features yield the highest accuracy, followed by the frequency features and acceleration, with the statistical feature being the least accurate.
3. It is worth noting that the acquisition of time-frequency features can be a complex process and may give rise to mode aliasing issues. Alternatively, the frequency features, which is readily obtainable and provides a certain level of accuracy assurance, can be selected as the preferred input for bridge seismic damage identification.

Acknowledgments

This research is supported by Guangxi Key Research and Development Program (Grant No. AB22036007).

ORCID

Xiaohang Zhou https://orcid.org/0000-0002-5040-8368
Yian Zhao https://orcid.org/0009-0005-6792-2696
Inamullah Khan https://orcid.org/0000-0002-5810-3585
Lu Cao https://orcid.org/0009-0009-0290-6467

References

Cao H, Friswell MI (2009) The effect of energy concentration of earthquake ground motions on the nonlinear response of RC structures. *Soil Dynamics and Earthquake Engineering* 29(2):292-299, DOI: 10.1016/j.soildyn.2008.02.003

Chicco D, Warrens MJ, Jurman G (2021) The coefficient of determination R-squared is more informative than SMAPE, MAE, MAPE, MSE and RMSE in regression analysis evaluation. *PEERJ Computer*

Science 7:e623, DOI: 10.7717/peerj-cs.623

Chiou JS, Jheng YW, Hung HH (2019) Numerical simulation of bridge piers with spread footings under earthquake excitation. *Earthquakes and Structures* 16(6):691-704, DOI: 10.12989/eas.2019.16.6.691

Deng T, Huang J, Cao M, Li D, Bayat M (2021) Seismic damage identification method for curved beam bridges based on wavelet packet norm entropy. *Sensors* 22(1):239, DOI: 10.3390/s22010239

Grave É, Joulin A, Cissé M, Grangier D, Jégou H (2017) Efficient softmax approximation for GPUs. Proceedings of 34th international conference on machine learning, August 6-11, Sydney, Australia

He Y, Chen H, Liu D, Zhang L (2021b) A framework of structural damage detection for civil structures using fast Fourier transform and deep convolutional neural networks. *Applied Sciences* 11(19):9345, DOI: 10.3390/app11199345

He HX, Zheng JC, Liao LC, Chen YJ (2021a) Damage identification based on convolutional neural network and recurrence graph for beam bridge. *Structural Health Monitoring* 20(4):1392-1408, DOI: 10.1177/1475921720916928

Jiao C, Li J, Wei B, Long P, Xu Y (2019) Experimental investigations on seismic responses of RC circular column piers in curved bridges. *Earthquakes and Structures* 17(5):435-445, DOI: 10.12989/eas.2019.17.5.435

Johnson GR, Cook WH (1983) A constitutive model and data for metals subjected to large strain, high strain rates and high temperatures. Proceedings of 7th International Symposium on Ballistics, April 19-21, Netherlands

Li D, Cao M, Deng T, Zhang S (2019) Wavelet packet singular entropy-based method for damage identification in curved continuous girder bridges under seismic excitations. *Sensors* 19(19):4272, DOI: 10.3390/s19194272

Liu L, Zhang X, Lei Y (2023) Data-driven identification of structural damage under unknown seismic excitations using the energy integrals of strain signals transformed from transmissibility functions. *Journal of Sound and Vibration* 546:117490, DOI: 10.1016/j.jsv.2022.117490

Lu J, Chen X, Ding M, Zhang X, Liu Z, Yuan H (2019) Experimental and numerical investigation of the seismic performance of railway piers with increasing longitudinal steel in plastic hinge area. *Earthquakes and Structures* 17(6):545-556, DOI: 10.12989/eas.2019.17.6.545

Maas AL, Hannun AY, Ng AY (2013) Rectifier nonlinearities improve neural network acoustic models. Proceedings of 30th International Conference on Machine Learning, June 16-21, Atlanta, America

Ni YQ, Zhang FL, Xia YX, Au SK (2015) Operational modal analysis of a long-span suspension bridge under different earthquake events. *Earthquakes and Structures* 8(4):859-887, DOI: 10.12989/eas.2015.8.4.859

Scott BD, Park R, Priestley MJ (1982) Stress-strain behavior of concrete confined by overlapping hoops at low and high strain rates. *Journal Proceedings* 79(1):13-27, DOI: 10.14359/10875

Shinozuka M, Feng MQ, Kim HK, Kim SH (2000) Nonlinear static procedure for fragility curve development. *Journal of Engineering Mechanics* 126(12):1287-1295, DOI: 10.1061/(ASCE)0733-9399(2000)126:12(1287)

Sokolova M, Lapalme G (2009) A systematic analysis of performance measures for classification tasks. *Information Processing & Management* 45(4):427-437, DOI: 10.1016/j.ipm.2009.03.002

Spokoiny V, Dickhaus T (2015) Basics of modern mathematical statistics. Springer, Heidelberg, Germany, 11-17

Teng Z, Teng S, Zhang J, Chen G, Cui F (2020) Structural damage detection based on real-time vibration signal and convolutional neural network. *Applied Sciences* 10(14):4720, DOI: 10.3390/app10144720

Wu CS, Peng YX, Zhuo DB, Zhang JQ, Ren W, Feng ZY (2022) Energy ratio variation-based structural damage detection using convolutional neural network. *Applied Sciences* 12(20):10220, DOI: 10.3390/app122010220

Zhang Y, Miyamori Y, Mikami S, Saito T (2019) Vibration-based structural state identification by a 1-dimensional convolutional neural network. *Computer-Aided Civil and Infrastructure Engineering* 34(9):822-839, DOI: 10.1111/mice.12447

Zhang J, Zhang J, Teng S, Chen G, Teng Z (2022) Structural damage detection based on vibration signal fusion and deep learning. *Journal of Vibration Engineering & Technologies* 10(4):1205-1220, DOI: 10.1007/s42417-022-00438-7

Zhou W, Li H, Mao C, Mevel L, Ou J (2013) Seismic damage detection for a masonry building using aftershock monitoring data. *Advances in Structural Engineering* 16(4):605-618, DOI: 10.1260/1369-4332.16.4.605

Zou JZ, Yang JX, Wang GP, Tang YL, Yu CS (2021) Bridge structural damage identification based on parallel CNN-GRU. *Earth and Environmental Science* 626:012017, DOI: 10.1088/1755-1315/626/1/012017